State-space inflow modelling for lifting rotors with mass injection

K. Yu and D. A. Peters
Department of Mechanical Engineering
Washington University,
St Louis, USA

ABSTRACT

In the field of rotorcraft dynamics, it is significant that the induced inflow field is well understood and modeled. A large number of methodologies have been developed in the past years, among which the state-space model is recognised for its advantage in real-time simulation, preliminary design, and dynamic eigenvalue analysis. Recent studies have shown success in representing the induced flow field everywhere above the rotor plane even with mass source terms on the disk as long as they have zero net flux of mass injection when integrated over the disk. Nevertheless, non-zero net mass influx is expected in numerous situations, such as ground effect, tip drive rotors, etc; and the incapability of previous models limits the utilisation of the methodology in these cases. This work presents an extended potential-flow, state-space model derived from the potential-flow momentum equation by means of a Galerkin approach. The induced velocity and pressure perturbation are expanded in terms of closed-form, time-dependent coefficients and space-dependent associated Legendre functions and harmonics. Non-zero net mass flux terms are represented by the involvement of associated Legendre functions with equal degrees and orders. Validation, as well as discrepancies, of the inclusion of such terms is investigated. Numerical simulation of frequency response in axial and skew-angle flight is presented and compared with exact solutions obtained by the convolution integral. Also the study shows that, unlike other pressure distribution responses, non-zero mass influx exhibits a high sensitivity to the choice of the number of states in the velocity expansion. Error analyses are performed to show this sensitivity.

NOMENCLATURE

$\hat{a}_n^m$, a_n^m	velocity expansion coefficients
$\hat{b}_n^m$, b_n^m	velocity expansion coefficients
[D]	damping matrix
E	error norm
H_n^m	coefficients
I	imaginary number
K_n^m	Legendre constant
$\left[\tilde{\mathbf{L}}\right]$	influence coefficient matrix
[**M**]	mass matrix
m	order of Legendre function (harmonic number)
N	highest value of subscript n
N_e	highest value of subscript n with $m + n$ = even
n	degree of Legendre function (Polynomial number)
p	pressure (N/m^2)
P	pressure, nondimensionalised as $p/\rho V_\infty^2$
P_n^m , Q_n^m	associated Legendre functions
$\bar{P}_n^m$, $\bar{Q}_n^m$	normalised associated Legendre functions
R	rotor radius (m)
t	time (sec)
$\bar{v}$	velocity perturbation, nondimensionalised as $\delta\bar{v}/V_\infty$
$\bar{V}_t$	total velocity vector (ms^{-1})
$\delta\bar{v}$	velocity perturbation (ms^{-1})
V_∞	free-steam velocity (ms^{-1})
χ	inflow angle
δ_{ij}	Kronecker delta

Paper No. 2863. Manuscript received 20 December 2003, revised copy received, 12 March 2004, accepted 3 May 2004.

https://doi.org/10.1017/S0001924000005157 Published online by Cambridge University Press

Φ_n^m	pressure functions (potential functions)
$\nu, \eta, \bar{\psi}$	ellipsoidal co-ordinates
ρ	density of fluid (kg/m^3)
ρ_n^m	normalisation factors
$\varsigma_n^m, \quad \sigma_n^m$	change of variable constants
τ	time, nondimensionalised as $V_\infty t/R$
$\tau_n^{mc}, \ \tau_n^{ms}$	pressure expansion coefficients
$\hat{\xi}$	unit vector in upstream direction
Ψ_n^m	velocity potential functions

Operators

$\overset{*}{(\ )}$	$\equiv d(\ )/d\tau$
$\bar{\nabla}$	Laplace operator

Superscripts and Subscripts

$(\ )^c$	cosine terms
$(\ )^s$	sine terms
$(\ )^m$	harmonic number
$(\ )_n$	polynomial number
$(\ )_z$	axial component
$(\ )_r$	radial component
$(\ )_{\bar{\psi}}$	azimuthal component

1.0 INTRODUCTION

An understanding of the flow field during flight is necessary in order to make design improvements to the performance and maneuverability of a helicopter. This is a crucial topic in preliminary design and flight test. As with other topics in research, there is more than one approach to the understanding of the flow field. CFD is probably the most fundamental method available. Nevertheless, the flexibility of CFD is offset by the large computational effort and the difficulty in capturing free vorticity. Vortex lattice results are another approach with great utility, but they can often be computationally prohibitive for analyses that require real-time simulation or eigenvalues. In these cases, a finite-state model of the inflow is required. This paper concentrates on finite-state modeling.

Sissingh[1] first proposed a simple, first-harmonic inflow and lift distribution without any dependence on the radial position along the rotor blade. That model assumed an instantaneous relationship between perturbations of induced velocity and perturbations in thrust. Sissingh showed good correlation of predicted data with flight measurements. In the early 1970s, Ormiston and Peters[2] introduced the idea of expressing the induced flow in state-variable form. The first theory was a quasi-steady formulation with the assumption of a linear relationship between perturbations of inflow components and of rotor thrust. This formulation represents the induced flow by a truncated Fourier series and assembles a theory that relates the inflow field at blades to the lift and circulation developed on the blades. This significantly simplifies the analysis of dynamic inflow. Peters later extended this model to the unsteady condition[3] by addition of the apparent mass of the inflow distributions. Though good correlation was obtained at axial or edgewise flow, a transition between these conditions was not allowed by this model.

In the 1980s, Peters and Pitt developed a linear, unsteady theory that relates transient rotor loads to the overall transient response of the rotor induced flow field[4-6]. This model is based on unsteady potential flow theory with the assumption that the total pressure due to a velocity field can be formed by superimposing the unsteady pressure and the static pressure of that field. Even though this theory proved to be practical and easy to use with good correlations, it is a low-order approximation and is limited to only the crudest wake description of uniform flow with one simple gradient. In 1987, Peters and He[7] turned to a higher-harmonic theory of dynamic inflow. The pressure distribution, as well as the inflow field, is extended to include an arbitrary number of harmonics and an arbitrary number of radial functions per harmonic. This new model gives excellent correlation on the rotor disk plane and in a more detailed fashion than does the Pitt model. However, it obtains only the normal component of flow at the rotor disk and does not provide all three components of flow on and above the rotor disk plane. In addition, it cannot be applied to cases with mass injection at the rotor. In 2001, based on a two-dimensional model studied by Nelson[8], Morillo extended the Peters-He Model to include an additional set of functions, which enabled the new model to remove most of the limitations of the previous model[9].

No net mass flow terms were considered in these models. However, some rotors have tip jets or blade slats with suction or blowing. These require that mass be injected into the wake. Also, some representations of ground effect require a source potential on the ground plane. These two types of rotors could not be handled by the state-space models of that time. This research reviews and extends Morillo's work, rather than build an entirely new model, since a good correlation has already been established. Net mass flow components are considered in the flow field by presence of certain pressure terms. Numerical results are compared with those from the convolution integral, and in some special cases, an exact solution in closed-form. Also, the influence of the choice of number of states, including number of discontinuous functions and mass injection functions, is investigated through error analysis. Optimised results for individual pressure distributions of net mass influx are obtained and compared to results from the original formation.

2.0 ORIGINAL STATE-SPACE MODEL

The derivation of the original state-space model is given in detail in Ref. 9. An abridged rendering is given below. We start with the incompressible potential flow equations, continuity and momentum.

$$\bar{\nabla} \cdot \vec{v}_t = 0 \qquad \ldots (1)$$

$$\frac{\partial \vec{v}_t}{\partial t} + \left(\vec{v}_t \cdot \bar{\nabla}\right)\vec{v}_t = -\frac{\bar{\nabla} p}{\rho} \qquad \ldots (2)$$

The induced velocity, $\delta\vec{v}$, is assumed to be small compared to the free-stream velocity, V_∞, which is taken along the negative $\hat{\xi}$ axis

$$\vec{v}_t = -V_\infty \hat{\xi} + \delta\vec{v} \qquad \ldots (3)$$

Thus, Equation (2) linearises to:

$$\frac{\partial \delta\vec{v}_t}{\partial t} - V_\infty \frac{\partial \delta\vec{v}_t}{\partial \xi} = -\frac{\bar{\nabla} p}{\rho} \qquad \ldots (4)$$

In non-dimensional form, this becomes

$$\frac{\partial \bar{v}}{\partial \tau} - \frac{\partial \bar{v}}{\partial \xi} = -\bar{\nabla} P \qquad \ldots (5)$$

It is straightforward to show from Equation (5) and continuity that $\nabla^2 P = 0$. Thus, pressure is a potential function. It further follows that $\bar{v}$ can be written as the gradient of a velocity potential,

https://doi.org/10.1017/S0001924000005157 Published online by Cambridge University Press

$$\vec{v} = \bar{\nabla}\Psi \qquad \ldots (6)$$

where $\nabla^2\Psi = 0$.

Since we are looking for pressure functions that have discontinuities in pressure or lift across a circular disk (the former being lift sources and the latter being mass flux sources) it is natural to use a set of ellipsoidal coordinates for the solutions to Laplace equation, Φ_n^m .

3.0 EXTENDED STATE-SPACE MODEL

A state-space model is developed with velocity perturbation and pressure perturbation expanded in series such that

$$P = -\sum_{m=0}^{\infty}\sum_{n=m}^{\infty}\left(\tau_n^{mc}\Phi_n^{mc} + \tau_n^{ms}\Phi_n^{ms}\right) \qquad \ldots (7)$$

$$\vec{v} = \sum_{m=0}^{\infty}\sum_{n=m}^{\infty}\left(\hat{a}_n^m\bar{\nabla}\Psi_n^{mc} + \hat{b}_n^m\bar{\nabla}\Psi_n^{ms}\right) \qquad \ldots (8)$$

where

$$\begin{cases}\Phi_n^{mc} = \Phi_n^m\cos(m\bar{\psi}) = \bar{P}_n^m(\nu)\bar{Q}_n^m(i\eta)\mathrm{Cos}(m\bar{\psi})\\ \Phi_n^{ms} = \Phi_n^m\sin(m\bar{\psi}) = \bar{P}_n^m(\nu)\bar{Q}_n^m(i\eta)\mathrm{Sin}(m\bar{\psi})\end{cases} \qquad \ldots (9)$$

$$\begin{cases}\Psi_n^{mc} = \int_{\xi}^{\infty}\Phi_n^{mc}\,\mathrm{d}\xi\\ \Psi_n^{ms} = \int_{\xi}^{\infty}\Phi_n^{ms}\,\mathrm{d}\xi\end{cases} \qquad \ldots (10)$$

$\bar{P}_n^m(\nu)$ and $\bar{Q}_n^m(i\eta)$ are normalised associated Legendre function of the first and second kind, respectively,

$$\bar{P}_n^m = (-1)^m\frac{P_n^m(\nu)}{\rho_n^m} \qquad \ldots (11)$$

$$\bar{Q}_n^m = \frac{Q_n^m(i\eta)}{Q_n^m(i0)} \qquad \ldots (12)$$

with

$$\left(\rho_n^m\right)^2 = \int_0^1\left[P_n^m(\nu)\right]^2\mathrm{d}\nu = \frac{1}{2n+1}\frac{(n+m)!}{(n-m)!} \qquad \ldots (13)$$

$$Q_n^m(i0) = \begin{cases}\dfrac{\pi}{2}(-1)^{m+n+1}(i)^{n+1}\dfrac{(n+m-1)!!}{(n-m)!!} & n+m = even\\ (-1)^{m+n+1}(i)^{n+1}\dfrac{(n+m-1)!!}{(n-m)!!} & n+m = odd\end{cases} \qquad \ldots (14)$$

τ_n^{mc} and τ_n^{ms}, $\hat{a}_n^m$ and $\hat{b}_n^m$ are time-dependent pressure coefficients and velocity coefficients, respectively. These coefficients are governed by the final non-dimensionalised matrix-form momentum equation.

In order to obtain the final equations, Equations (7–8) are substituted into the nondimensional potential flow equations. Then, a Galerkin approach is applied. In particular, the equation is dotted from the left by $\bar{\nabla}\Phi_j^r$ and integrated over the upper-half space above the plane of the rotor. The Divergence Theorem is used to bring the integrals down to only integrals on the rotor disk, which can be done in closed form. The result is the following where all coefficients are known explicitly, Appendix A.

$$\left[\mathbf{M}^c\right]\left\{\dot{a}_n^m\right\} + \left[\mathbf{D}^c\right]\left[\tilde{\mathbf{L}}^c\right]^{-1}\left[\mathbf{M}^c\right]\left\{a_n^m\right\} = \left[\mathbf{D}^c\right]\left\{\tau_n^{mc}\right\} \qquad \ldots (15)$$
$$m = 0,1,2,3,\cdots, \quad n = m+1,\ m+2,\ m+3,\cdots.$$

The derivation of Equation (15) utilises a change of variable from $\hat{a}_n^m$ to a_n^m .

$$\left\{\Psi_n^{mc}\right\}^T\left\{\hat{a}_n^m\right\} = \left\{\sigma_n^m\Phi_{n+1}^{mc} + \varsigma_n^m\Phi_{n-1}^{mc}\right\}^T\left\{a_n^m\right\} \qquad \ldots (16)$$

where

$$\sigma_n^m = \frac{1}{K_n^m\sqrt{(2n+1)(2n+3)\left[(n+1)^2 - m^2\right]}} \qquad \ldots (17)$$

$$\varsigma_n^m = \frac{1}{K_n^m\sqrt{\left(4n^2-1\right)\left(n^2-m^2\right)}} \qquad n \neq m \qquad \ldots (18)$$

and

$$K_n^m = \left(\frac{\pi}{2}\right)^{(-1)^{n+m}}H_n^m \qquad \ldots (19)$$

$$H_n^m = \frac{(n+m-1)!!(n-m-1)!!}{(n+m)!!(n-m)!!} \qquad \ldots (20)$$

This change of variable allows the representation in Equation (10) to be known in closed form everywhere in the flow field.

Superscripts '*c*' in matrix notation imply these are cosine components of the complete equation. However, Equations (7-8) imply that the sine and cosine terms are completely decoupled, so an identical set of equations for sine components could be written. The spatial variables in an ellipsoidal coordinate system are shown in Fig. 1 where $\bar{\Psi}$ is the azimuthal angle measured counterclockwise from negative *x*-axis in *x*-*y* plane.

The state-space model represented by Equation (15) yields excellent correlation for all three components of velocity perturbations everywhere in the flow field above the rotor plane for various pressure distributions, which are determined uniquely by rotor conditions (i.e. number of blades, sectional lift, blades rotating frequency, etc). However, the net mass flow terms, which are presented by associated Legendre functions with equal orders and degrees, i.e., $m = n$, in pressure expansions, are not adopted in this formulation. This is based on the fact that these terms yield infinite kinetic energy in the flow field, as shown below.

Without losing generality, assume a pressure distribution $P = -\Phi_0^0$ The vertical component of induced velocity yields

$$v_z = \Phi_0^0 = \bar{P}_0^0(\nu)\bar{Q}_0^0(i\eta) \qquad \ldots (21)$$

https://doi.org/10.1017/S0001924000005157 Published online by Cambridge University Press

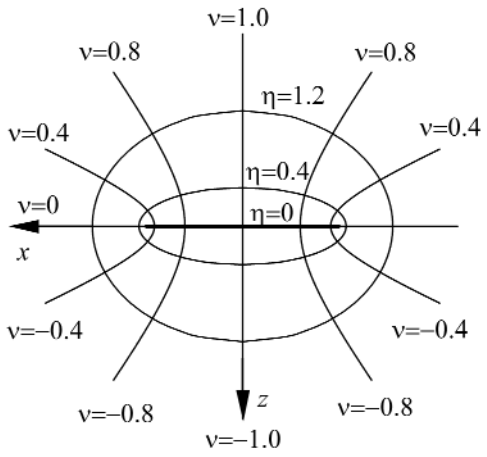

Figure 1. Ellipsoidal coordinates viewed in x-z plane

and therefore, on the upper surface of the plane of the disk

$$v_z = \begin{cases} \bar{P}_0^0(v) = 1 & \text{on-disc} \\ \bar{Q}_0^0(i\eta) = \frac{2}{\pi}\mathrm{Tan}^{-1}\left(\frac{1}{\eta}\right) & \text{off-disc} \end{cases} \quad \ldots (22)$$

There is, of course, a jump for below the disk.

For the off-disk area in the plane of the disk, and if a Taylor series is used for large η

$$v_z = \frac{2}{\pi}\mathrm{Tan}^{-1}\left(\frac{1}{\eta}\right) = \frac{2}{\pi}\left(\frac{1}{\eta} - \frac{1}{3\eta^3} + \cdots\right) \quad \ldots (23)$$

then the kinetic energy per unit area crossing the off-disk rotor plane ($v = 0$, $a \le \eta < \infty$) is that

$$T = \frac{1}{2}\iint_s v_z^2 \mathrm{d}s = \frac{4}{\pi}\int_a^\infty \left(\frac{1}{\eta} - \frac{1}{3\eta^3}\right)^2 \eta \mathrm{d}\eta = \infty \quad \ldots (24)$$

Equation (24) fully expresses the major problem with including non-zero net mass flux terms in the model. In particular, the involvement of net mass flux terms, which happens in practical cases, will theoretically introduce infinite energy in the flow field. However, the infinite result only occurs if the media field does not dissipate energy at all, and if the whole system, including the media field, is taken to a distance of infinity. In reality, damping of air, even though very small under the conditions of helicopter operation, will dissipate the energy; and the induced velocity decreases much faster away from the rotor than shown in Equation (23). Secondly, the operating period of a helicopter is not infinite. Furthermore, the study of induced flow is not the final goal in the study of helicopter performance — the ultimate goal is to see how it affects the behaviour of helicopter blades, fuselage or personnel on the ground if it is close to the ground. Therefore, the most important concern is the area on or close to the actuator disk, not in the far field. Based on this aspect, if the results have good correlation in the on-disk, or close-to-disk, area, the involvement of net mass flux could be tolerated.

The variable change shown in Equation (16) prohibits any $m = n$ terms in the velocity expansion in Equation (8). However, this prohibition is only for the mass matrix $[\mathbf{M}^c]$ and the influence coefficient matrix $[\tilde{\mathbf{L}}^c]$ and has no bearing on the matrix $[\mathbf{D}^c]$, which is the coefficient matrix of the pressure coefficients on the right-hand-side of Equation (15). Therefore, it might be possible to include $m = n$ in τ_n^m without introducing corresponding velocity potentials of the same order.

The justification for this is as follows. There are no singularities or mathematical difficulties in including Φ_m^m in the pressure function on the right-hand side. These are valid solutions to Laplace's equation that satisfy the boundary conditions. Although it is tempting to add a parallel set of functions to the velocity potential, Ψ_m^m, such that $\partial\Psi_m^m/\partial z = \Phi_m^m$, such functions would involve Φ_{m-1}^m , Equation (16), which is not defined, and this results in singularities in the matrices that are due to the infinite kinetic energy. Therefore, we add Φ_m^m but do not take any Ψ_m^m terms.

To include net mass flux terms, i.e. $\bar{P}_m^m(v)$ and $\bar{Q}_m^m(i\eta)$, in the pressure distribution, the damping coefficient matrix $[\mathbf{D}^c]$ on the right hand side of Equation (15) will be required to have extra columns. Based on the goal that the new model should reduce to Equation (15) if net mass flux terms are not considered, these new entrees are desired to follow the same formulation of $[\mathbf{D}^c]$. The formulation in Appendix A indeed does not exclude any equal degree-order associated Legendre functions either in its closed-form representation or derivation; and therefore, the net mass flux terms could be included in the pressure distribution. The extended momentum equation is thus expressed as

$$\left[\mathbf{M}^c\right]\left\{\dot{a}_n^m\right\} + \left[\mathbf{D}^c\right]\left[\tilde{\mathbf{L}}^c\right]^{-1}\left[\mathbf{M}^c\right]\left\{a_n^m\right\} = \left[\bar{\mathbf{D}}^c\right]\left\{\tau_n^{mc}\right\} \quad \ldots (25)$$

where $[\bar{\mathbf{D}}^c]$ is the extended matrix to include $n = m$. Equation (25) is now the extended dynamic wake model.

4.0 ERROR ANALYSIS AND SIMULATION

The validity of the proposed state-space model, Equation (25), is investigated by an error analysis. In this study, error is defined by

$$E^2 = \frac{\int_A^B \left(\left|v_s - v_e\right|^2 / \sqrt{1+\eta^2}\right) dr}{\int_A^B \left(\left|v_e\right|^2 / \sqrt{1+\eta^2}\right) dr} \quad \ldots (26)$$

where v_s and v_e are velocity perturbations from state-space model and convolution/closed-form solution, respectively, r is the radial location, and A and B are the range of desired area of investigation. Since the accuracy of the model is of less importance off the disk, errors are multiplied by the weight coefficient $1/\sqrt{1+\eta^2}$. Therefore, the further from the disk, the less error is counted in the analysis. From this point, for the sake of convenience, $m + n$ = even and $m + n$ = odd terms will be called 'even' and 'odd' terms, respectively.

It should be noted that optimum truncation strategies are discussed in detail in Ref. (9). Basically, that reference shows that in axial flow, the number of even and odd terms should be equal, with even terms dropped as skew angle increases until no even terms are present when $\chi = 90°$. We take basically this same strategy here, but with some studies as to whether the old strategy needs to be modified in any way to accommodate the new mass injection terms.

The previous Peters-He state-space model yields the exact solution at edge-wise inflow if there are no even terms in the velocity expansion. Morillo expanded the model to include mass injection terms in the pressure expansion, which demands involvement of even as well as odd terms in velocity. It is intuitive that the number of even terms will change the correlation with the exact solution. Verification of this assumption is done by error analyses with various numbers of even terms in the state-space model. In this study, the number of even and odd terms is represented by the number of terms in the zeroth harmonic, that is, how many odd or even terms with $m = 0$ are included.

https://doi.org/10.1017/S0001924000005157 Published online by Cambridge University Press

For all of the illustrations shown, the pressure distribution is such that

$$P = -\Phi_m^{mc} = -\bar{P}_m^m(\nu)\bar{Q}_m^m(i\eta)\cos(m\bar{\psi}) \quad \ldots (27)$$

To examine the generality of the proposed model, various excitation frequencies, as well as skew angles along with different pressure distribution, are evaluated and discussed.

Figure 2 shows an example of error analysis for the pressure distribution $P = -\Phi_0^0$ with zero and infinite frequencies during axial flow. In this case, N and N_e represent the highest subscripts of Φ_n^m for odd terms and for even terms, respectively. Thus, there are roughly half as many odd (or even) terms as the value of N (or N_e). Figure 2(a) shows the analysis with equal numbers of odd and even terms in the model, while Fig. 2(b) shows the effect of number of even terms in the model as the number of odd terms is fixed at 11. From Figs 2(a) and 2(b), it is shown that the precision of results follows a rather smooth trend within a certain range of number of states that yields convergence. Within that range, the precision intends to increase with more terms included. Numerical simulation verifies that, beyond the range of convergence, (for example, number of states greater than 20 as shown in 2(a)), the convergence starts to break down and collapse rapidly if the number of states goes even higher. However, Figs 2(c) and 2(d) do not follow this same pattern. The accuracy of simulation oscillates with change in the number of states. This is because the case $\omega = \infty$ is the far limit of applicability which can never be approached in practice. The $\omega = \infty$ case has extreme singularities of the rotor edge which are not well modeled by a Galerkin approach.

Figures 2(e) and 2(f) give the errors with frequency $\omega = 2{\cdot}3$. Plots show that the error becomes, in general, smaller and smaller with increase in the number of states. In other words, the error analysis suggests that the convergence of the model is not monotonic with respect to the number of states adopted in the model — it depends on both the number of states of choice and frequency/skew-angle of flight. Other simulation results verify that increase of frequency or skew angle shrinks the range of convergence. If the skew angle is changed, the number of even terms included becomes more and more important to the model's convergence. Some of these phenomena, like the effect of skew angle on convergence, agree with that of zero net mass flow pressure distributions.

Figures 3–8 illustrate the on-disk optimised frequency responses

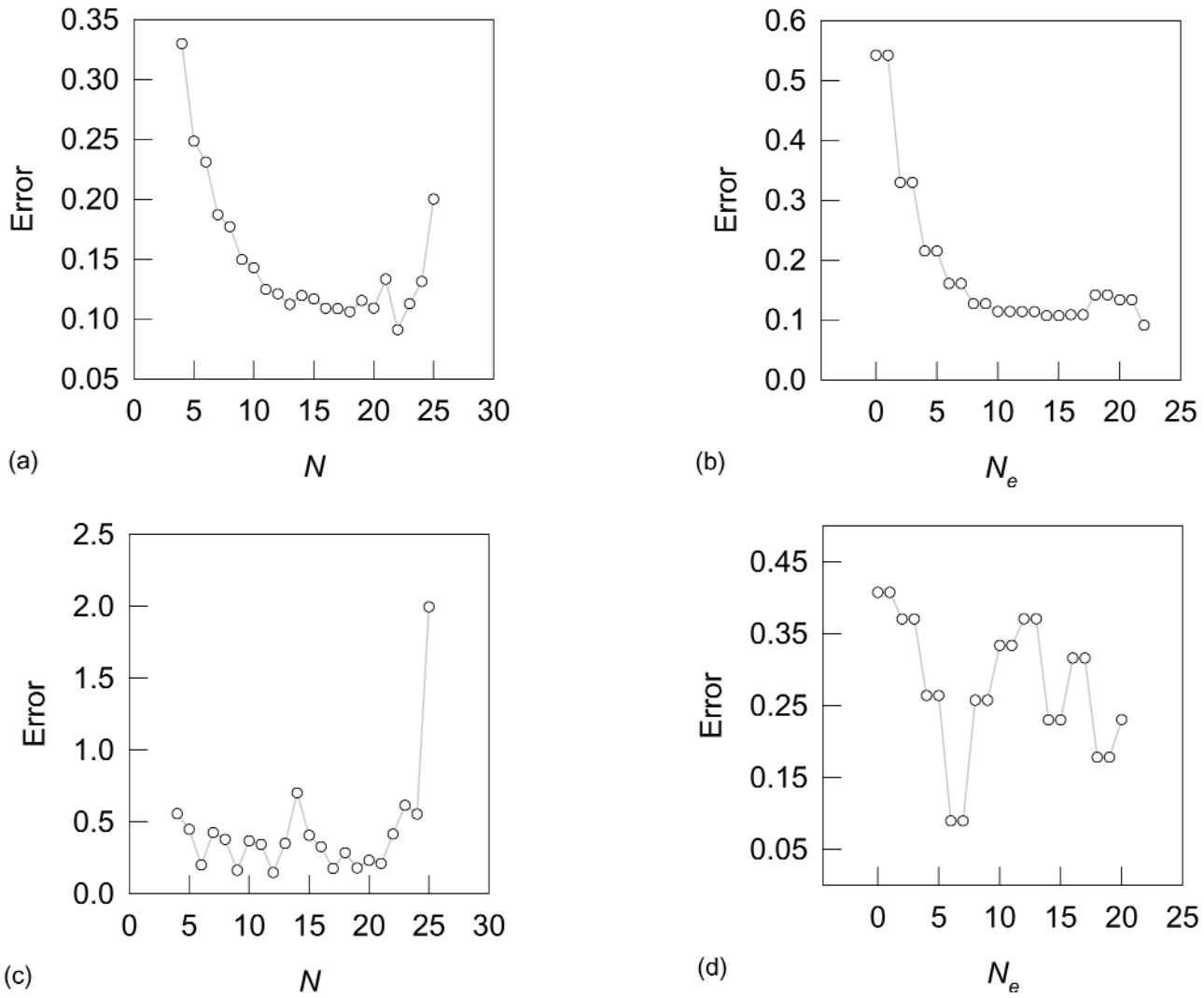

Figure 2. On-disc error analysis comparing results from state-space model and convolution integral. Pressure distribution $P = -\Phi_0^0$ with $\omega = 0$ ((a) and (b)), $\omega = \infty$ ((c) and (d)) and $\omega = 2{\cdot}3$ ((e) and (f)). The state-space model in (a), (c) and (e) uses various but equal numbers of even and odd terms (N) in the zeroth harmonic; In (b) it has 22 odd terms and various number of even terms (N_e) in the zeroth harmonic; In (d) it has 20 odd terms and various number of even terms (N_e) in the zeroth harmonic; In (f) it has 25 odd terms and various number of even terms (N_e) in the zeroth harmonic. Responses are evaluated with $z = 0$ (on the actuator plane), $x = 0$ (axial inflow), $\psi = 0$, 180 (along fore-and-aft axis).

https://doi.org/10.1017/S0001924000005157 Published online by Cambridge University Press

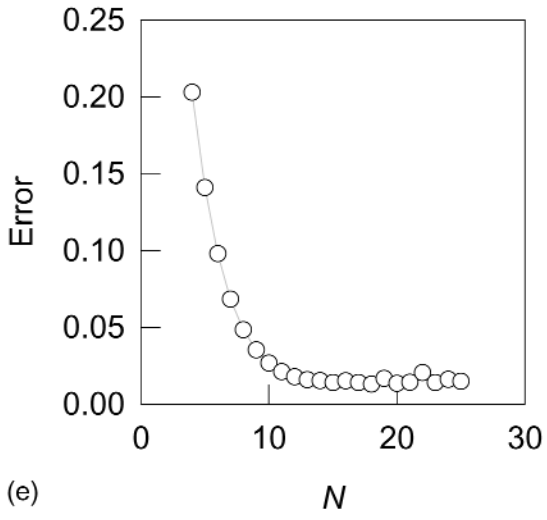

Figure 2(e).

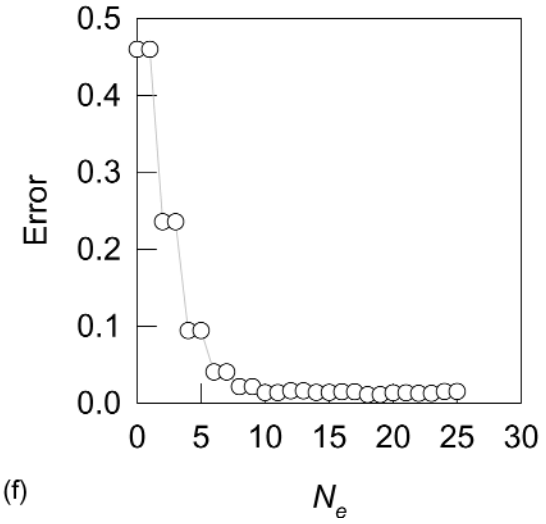

Figure 2(f).

of pressure distribution $P = -\Phi_0^0$ with various system configurations. In all plots, circles are results from a closed-form convolution integral, Appendix B; triangles are results from closed-form solutions, which are available in limited cases; and dots represent results of the proposed state-space model from the Galerkin approach.

From Figs 2(a) and 2(b), it is observed that, when the odd terms and even terms are each 11 in the zeroth harmonic, the state-space model yields the highest accuracy for the zero frequency response with respect to the exact solution. Numerical verification, plotted in Fig. 3 shows that, even though this is the optimal choice, visible errors still exist in both on-disk and off-disk area. As discussed, the velocity expansion includes no terms with $m = n$. Notice if the pressure distribution is $P = -\Phi_0^0$, from Equation (16), the closed-form solution of the z-component of on-disk velocity perturbation is uniform. However, there is no function in the velocity expansion that has property of being uniform on-disk. Therefore, it requires a large number of terms in the velocity expansion to yield a good approximation. On the other hand, error analysis suggests that the convergence collapses after the number of states goes beyond a certain range. These two facts contribute to this error shown in Fig. 3(a). On the off-disk area, the Galerkin approach decays into the far field faster than the exact solution. This is expected and has been discussed in the previous section on infinite kinetic energy.

Figure 4 is the frequency response for an infinite frequency. Based on the fact that the response actually becomes zero in this case, ωv_i, $i = z, r, \bar{\psi}$ is plotted. It shows that the on-disk and far off-disk areas have good correlation with the exact solution, yet relatively large oscillations appear at the edge of actuator. This is a consequence of the singularity at the disk edge when $\omega = \infty$.

Figure 5 is the optimised state-space simulation with frequency at ω = 2·3, and it exhibits excellent correlation with convolution results. The total number of odd and even terms is 12 and 10, respectively. The error analysis indicates about 1% error.

Based on individual error analyses, optimised results of frequency response under various conditions are obtained and plotted in Figs 6–8. Figure 6 shows the response one disk radius above the rotor plane in axial flow. Again it is noticed that the error is consistent, but it is of the same order as the off-disk error in Fig. 2(a). The fact that our shape functions cannot die out as $1/r$ whereas the true v_z does,

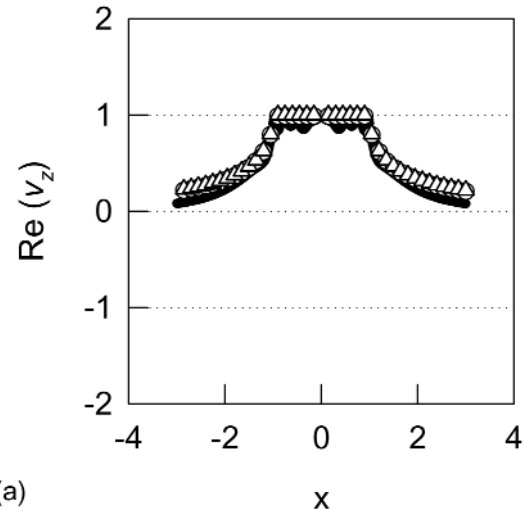

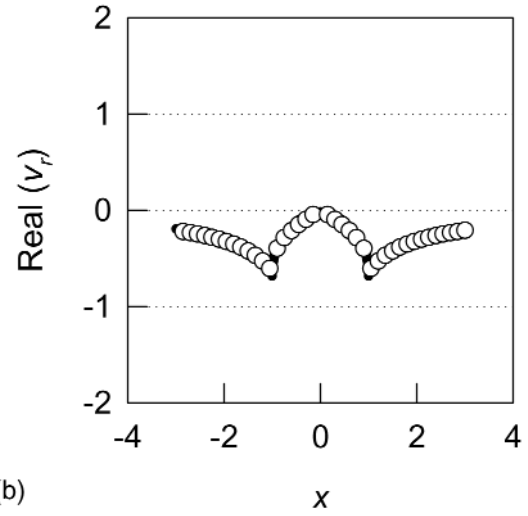

Figure 3. Frequency response of pressure distribution $P = -\Phi_0^0$ with $\omega = \infty$. All other components of induced velocities are zeroes. Both number of odd and even terms included in state-space model are 11. Highest power of radial polynomials is 22. Responses are evaluated with $z = 0$ (on the actuator plane), $\chi = 0$ (axial inflow), $\psi = 0$, 180 (along fore-and-aft axis). Circles present values of convolution integral results at locations; triangles present results of closed-form solution; and dots present results obtained by Galerkin approach.

https://doi.org/10.1017/S0001924000005157 Published online by Cambridge University Press

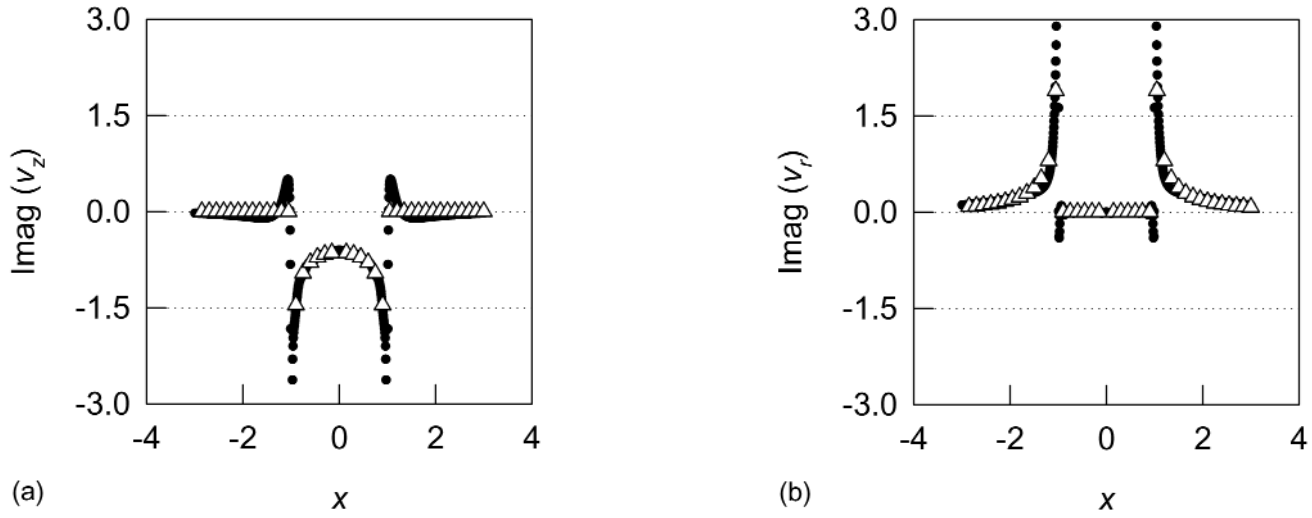

Figure 4. Frequency responses of pressure distribution $P = -\Phi_0^0$ with $\omega = \infty$. All other components of induced velocities are zeroes. Number of odd terms included in the state-space model is 10; Number of even terms is 3. Highest power of radial polynomials is 20. Responses are evaluated with $z = 0$ (on the actuator plane), $\chi = 0$ (axial inflow), $\psi = 0$, 180 (along fore-and-aft axis). Triangles present results of closed-form solution; and dots present results obtained by Galerkin approach.

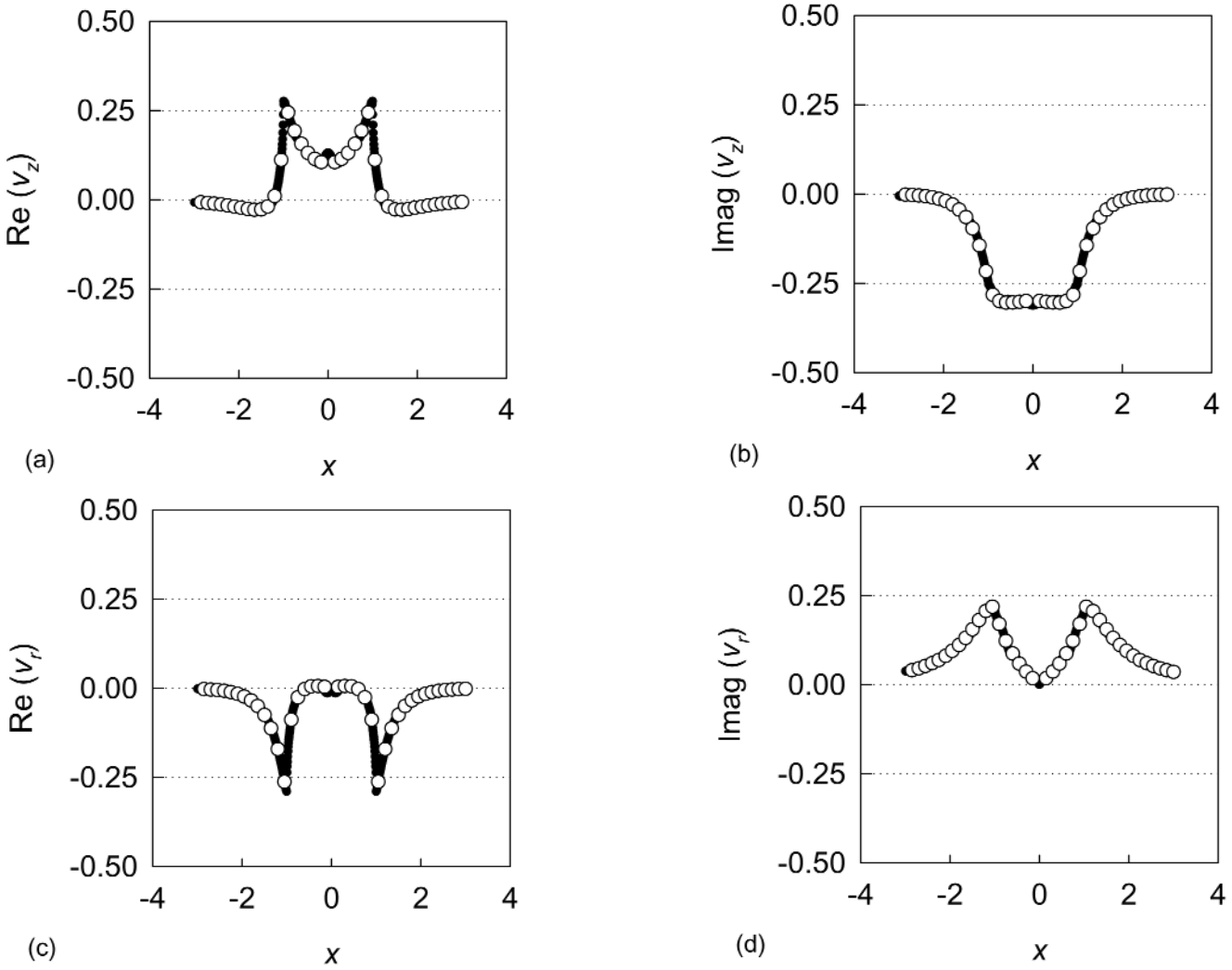

Figure 5. Frequency responses of pressure distribution $P = -\Phi_0^0$ with skew angle $\chi = 0$, frequency $\omega = 2 \bullet 3$. Number of odd terms is 25; number of even terms is 20. Highest power of radial polynomials is $N_r = 25$. Evaluation is performed on the actuator plane, $z = 0$. Plots (a) and (b) are real and imaginary parts, respectively, of vertical component of induced velocity. Plots (c) and (d) are those of radial component of induced velocity. Circles present values of convolution integral results at locations; and dots present results obtained by Galerkin approach.

https://doi.org/10.1017/S0001924000005157 Published online by Cambridge University Press

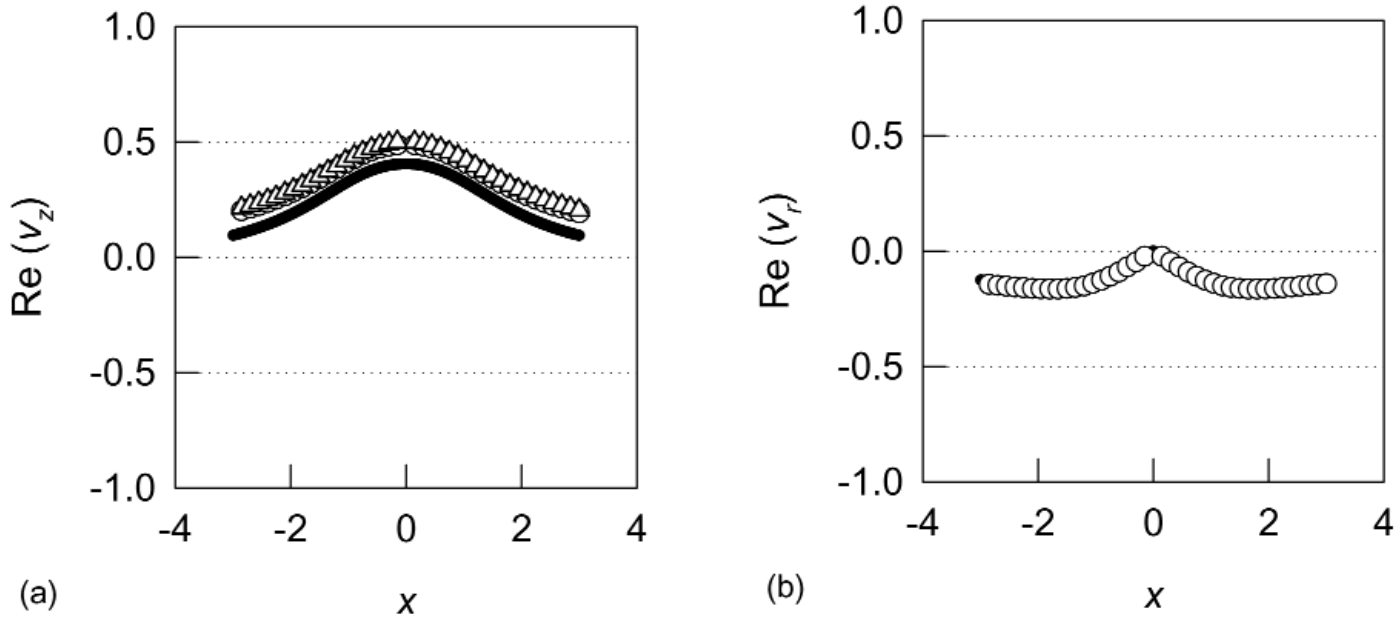

Figure 6. Frequency response of pressure distribution $P = -\Phi_0^0$ with $\omega = 0$. All other components of induced velocities are zeroes. Both number of odd and even terms included in state-space model are 11. Responses are evaluated with $z =$ 1 (one radius above the actuator plane), $\chi = 0$ (axial inflow), $\psi = 0$, 180 (along fore-and-aft axis). Circles present values of convolution integral results at locations; triangles present results of closed-form solution; and dots present results obtained by Galerkin approach.

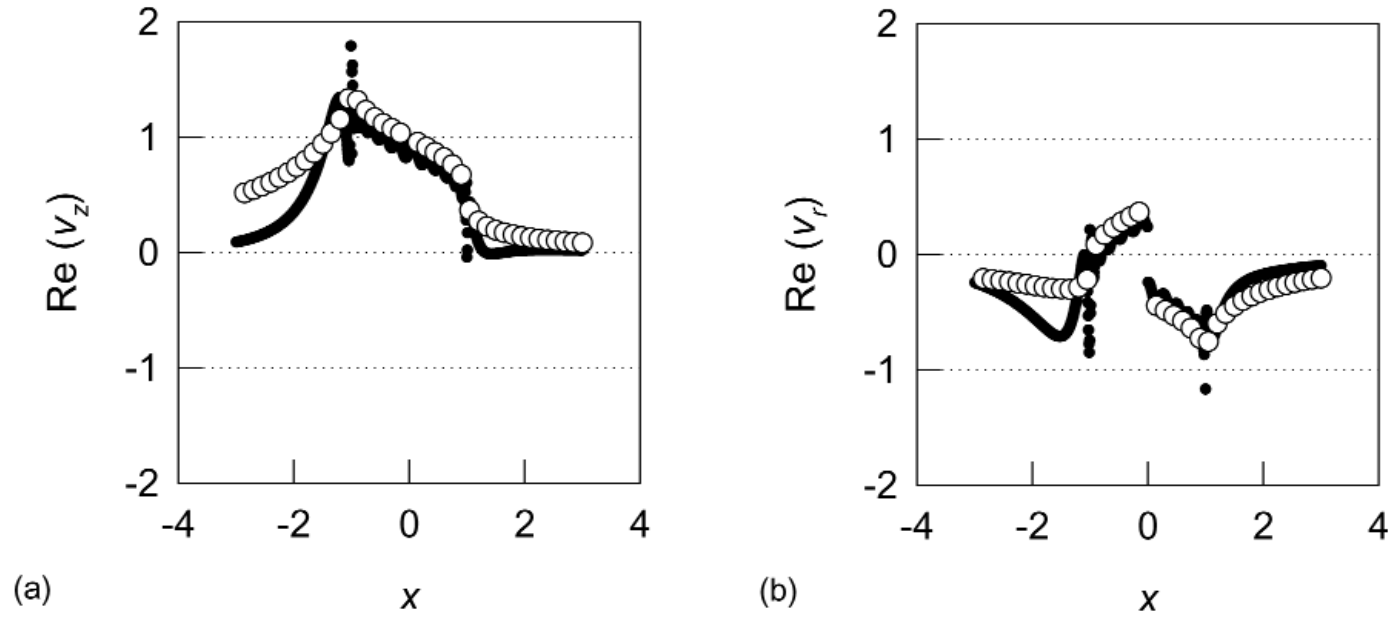

Figure 7. Frequency responses of pressure distribution $P = -\Phi_0^0$ with $\omega = 0$. All other components of induced velocities are zeroes. Number of odd terms included in the state-space model is 12; Number of even terms is 5. Highest power of radial polynomials is 24. Responses are evaluated with $z = 0$ (on the actuator plane), $\chi = 45$, $\psi = 0$, 180 (along fore-and-aft axis). Circles present results of convolution integral; and dots present results obtained by Galerkin approach.

explains why v_z is underestimated at one radius above the disk.

Figure 7 shows the response at zero frequency in skewed flight. Considering that the vortices do not die out in the skewed wake, the induced flow will be larger in the trailing edge. Morillo showed that, in skewed flow, the number of even terms should be reduced to obtain optimum convergence. However, it is also desired to have a certain number of even terms in the velocity expansion because of the inclusion of even terms in the pressure distribution. A compromise can be found, but the error off-disk especially at the trailing edge is amplified. The accuracy of the model is evaluated on-disk in this research; and, indeed, Fig. 6 shows this. In further research, an over-all error analysis could be performed to find another optimised number of states to give better correlation off-disk, with certain accuracy loss in the on-disk area.

Figure 8 shows response at a higher frequency, skewed-angle flight. Figure 8 shows good correlations in all four non-zero components. This is a direct result of increase of excitation frequency. For any non-zero frequency, the response is of the form

https://doi.org/10.1017/S0001924000005157 Published online by Cambridge University Press

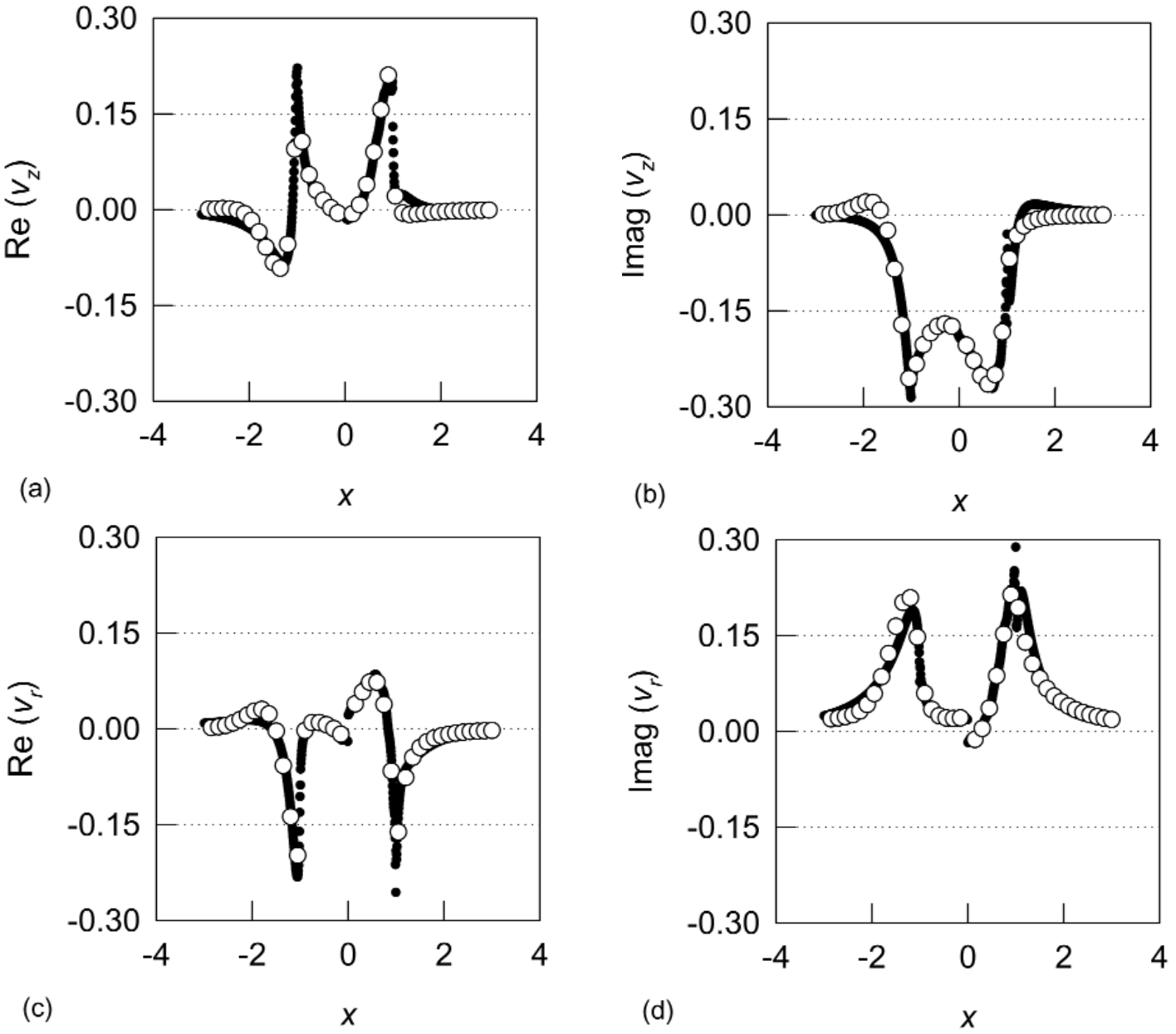

Figure 8. Frequency responses of pressure distribution $P = -\Phi_0^0$ with skew angle $\chi = 45$, frequency $\omega = 4$. Number of odd terms is 12; number of even terms is 4. Highest power of radial polynomials is $N_r = 24$. Evaluation is performed on the actuator plane, $z = 0$. Plots (a) and (b) are real and imaginary parts, respectively, of vertical component of induced velocity. Plots (c) and (d) are those of radial component of induced velocity. Circles present values of convolution integral results at locations; and dots present results obtained by Galerkin approach.

$$\{\bar{\mathbf{x}}\} = [\mathbf{B} + i\omega\mathbf{A}]^{-1}\{\bar{\mathbf{o}}\} \qquad \ldots \quad (28)$$

and the error, if any, is decreased by factor of

$$\kappa = \frac{|\mathbf{B}|}{|i\omega\mathbf{A} + \mathbf{B}|} \qquad \ldots \quad (29)$$

as long as ω does not approach infinity.

As long as the state-space model is within convergence range, the increase of frequency always plays a role in reducing the error. This also explains the excellent correlation shown in Fig. 5.

For purposes of illustration of generality of the model, Figs 9 and 10 are presented to show the responses of pressure distribution $P = -\Phi_1^1 \cos\Psi$ with zero and infinite frequencies. From all the plots, it can be seen that the radial components always have good correlation with the exact solution, even when the axial components yield large error. The errors for Φ_1^1 are less than those for Φ_0^0.

5.0 CONCLUSIONS

It is shown that the proposed state-space model is capable of treating non-zero net mass flux terms in the pressure distribution. Validation is performed through error analyses and numerical verification. Based on the results obtained, the following conclusions are made

The proposed state-space model with the extended damping matrix is capable of including non-zero mass flux terms in the pressure distribution. The fact that these terms yield infinite kinetic energy is considered. Numerical results nevertheless agree with exact solutions for practical applications.

https://doi.org/10.1017/S0001924000005157 Published online by Cambridge University Press

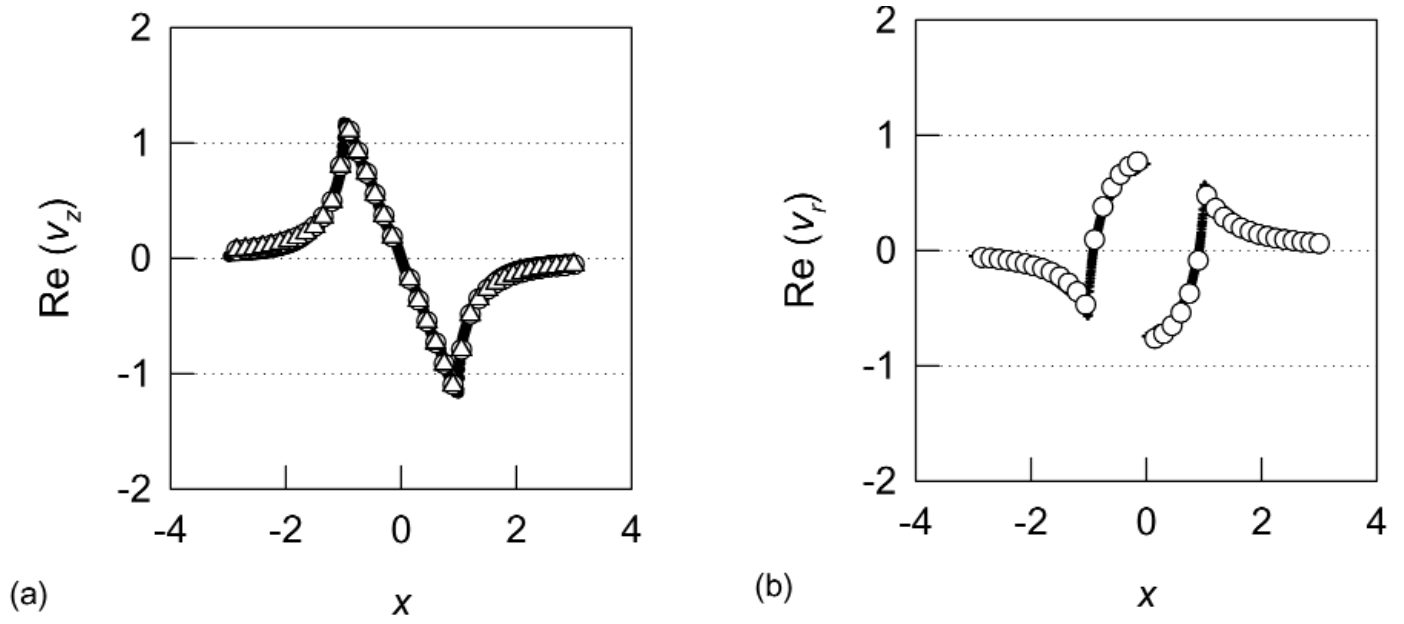

Figure 9. Frequency response of pressure distribution $P = -\Phi_1^1$ with $\omega = 0$. All other components of induced velocities are zeroes. Numbers of odd and even terms included in state-space model are 11 and 10, respectively. Highest power of radial polynomial is 21. Responses are evaluated with $z = 0$ (on the actuator plane), $\chi = 0$ (axial inflow), $\psi = 0$, 180 (along fore-and-aft axis). Circles present values of convolution integral results at locations; triangles present results of closed-form solution; and dots present results obtained by Galerkin approach.

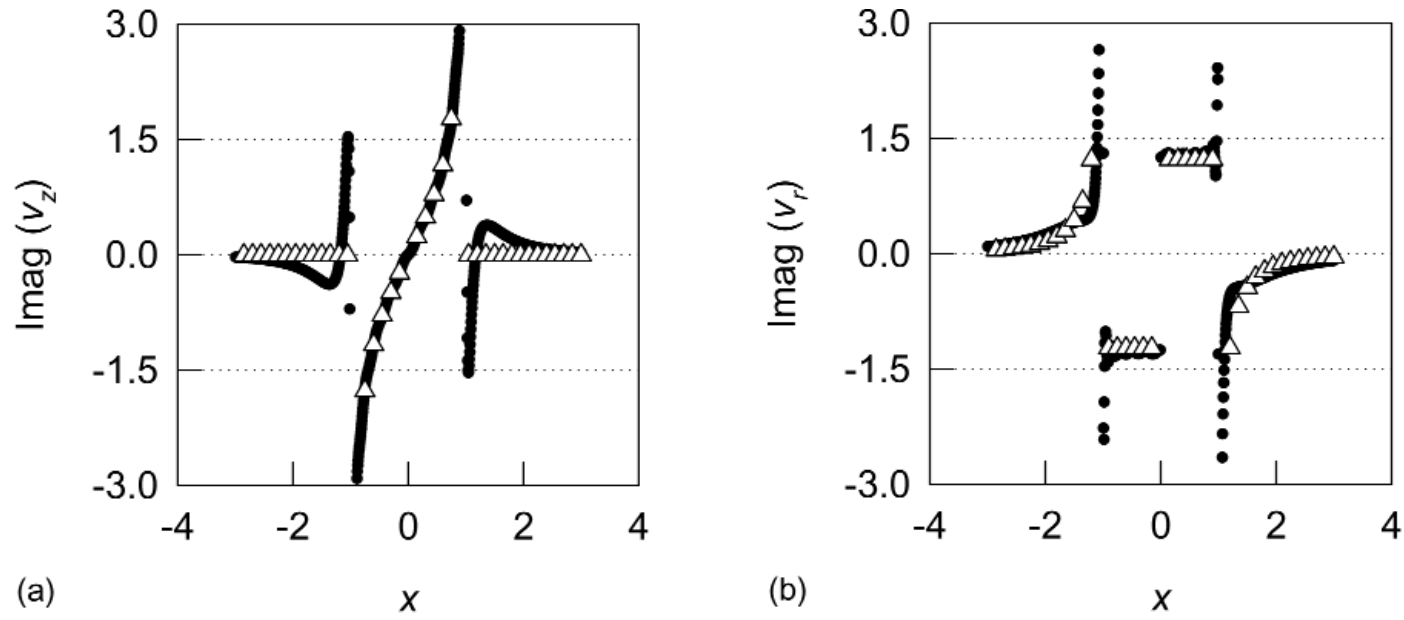

Figure 10. Frequency response of pressure distribution $P = -\Phi_1^1$ with $w = \infty$. All other components of induced velocities are zeroes. Numbers of odd and even terms included in state-space model are 12 and 4, respectively. Highest power of radial polynomial is 23. Responses are evaluated with $z = 0$ (on the actuator plane), $\chi = 0$ (axial inflow), $\psi = 0$, 180 (along fore-and-aft axis). Circles present values of convolution integral results at locations; triangles present results of closed-form solution; and dots present results obtained by Galerkin approach.

The convergence of the model is not ideal with low frequency or large skew-angle flight. Error on the trailing edge becomes significant in these cases.

A trade-off sometimes exists during optimization. The choice of number of states is based on the importance of location of induced flow. On-disk optimization usually gives excellent correlation on-disk, but loses convergence off-disk. If an overall optimisation is adopted, the excellence of on-disk correlation will be reduced.

Other adjustments and calibrations are always of interest to improve the proposed model. However, a major future work is to apply the complete state-space model with blade element theory and blade dynamics, and experimented results if available, to verify the complete validity of model.

ACKNOWLEDGEMENT

This work was sponsored by the Army Research Office, Agreement #DAAD19-01-1-0697, Tom Doligalski, Technical Monitor.

https://doi.org/10.1017/S0001924000005157 Published online by Cambridge University Press

REFERENCES

1. SISSINGH, G. J. The effect of induced velocity variation on helicopter rotor damping in pitch or roll, 1952, Aeronautical Research Council (Great Britain), ARC Technical Report CP No 101 (14,757).
2. ORMISTON, R.A. and PETERS, D.A. Hingeless helicopter rotor response with non-uniform inflow and elastic blade bending, *J Aircr*, **9,** (10), O. 1972, pp 730-736.
3. PETERS, D.A. Hingeless rotor response with unsteady flow, presented at the AHS/NASA-Ames Specialists Meeting on Rotorcraft Dynamics, NASA SP-362, February 1974.
4. PITT, D.M. Rotor Dynamic Inflow Derivatives and Time Constant from Various Inflow Models, Doctor of Science Thesis, Washington University, December 1980.
5. PITT, D.M. and PETERS, D.A. Theoretical prediction of dynamic inflow derivative, March 1981, *Vertica*, **5,** (1), pp 21-34.
6. PITT, D.M. and PETERS, D.A. Rotor dynamic inflow derivatives and time constants from various inflow models, 9th European Rotorcraft Forum, Stresa, Italy, 13-15 September, 1983.
7. PETERS, D.A. and HE, C-J. A finite-state induced-flow model for rotors in hover and forward flights, proceedings of the 43rd Annual National Forum of the American Helicopter Society, St Louis, MO, May 1987.
8. NELSON, A.M. A State-Space, Two-Dimensional Potential Flow Wake Model from a Galerkin Approach, May 2001, Master of Science Thesis, Washington University.
9. MORILLO, J.A. A Fully Three-Dimensional Unsteady Rotor Inflow Model from a Galerkin Approach, December 2001, Doctor of Science Thesis, Washington University.
10. HE, C-J. Development and Application of a Generalized Dynamic Wake Theory for Lifting Rotors, July 1989, Doctor of Philosophy Thesis, Georgia Institute of Technology.
11. GAUTSCHI, W. Computational aspects of three-term recurrence relations, *SIAM Review*, **9,** 1967, pp 24-82.
12. GRADSHTEYN, I.S. and RYZHIK, I.M. *Table of Integrals, Series, and Products*, Academic Press, New York, 1980.
13. ABRAMOWITZ, M. and STEGUN, I.A. *Handbook of Mathematical Functions*, Dover Publications, New York, 1970.

APPENDIX A: CLOSED-FORM COEFFICIENTS

1. Mass matrix [M]

$$M_{jn}^{rm} = \frac{2}{\sqrt{H_n^m H_j^m}} \frac{(-1)^{\frac{n+j-2m}{2}} \sqrt{(2n+1)(2j+1)}}{(n+j)(n+j+2)\left[(n-j)^2-1\right]} \qquad (A.1)$$
$$r = m, \quad j+r = \text{odd}, \quad n+m = \text{odd}$$

$$M_{jn}^{rm} = \frac{8}{\pi^2 \sqrt{H_n^m H_j^m}} \frac{(-1)^{\frac{n+j-2m+2}{2}} \sqrt{(2n+1)(2j+1)}}{(n+j)(n+j+2)\left[(n-j)^2-1\right]} \qquad (A.2)$$
$$r = m, \quad j+r = \text{even}, \quad n+m = \text{even}$$

$$M_{jn}^{rm} = \frac{1}{\sqrt{H_n^m H_j^m}\sqrt{(2n+1)(2j+1)}} \qquad (A.3)$$
$$r = m, \quad j+r = \text{even}, \quad n+m = \text{odd}$$
$$r = m, \quad j+r = \text{odd}, \quad n+m = \text{even}$$

$$M_{jn}^{rm} = 0 \qquad (A.4)$$
$$r \neq m$$

2. Damping matrix [D]

$$D_{jn}^{rm} = \frac{1}{K_n^m}\delta_{jn} \qquad (A.5)$$
$$r = m, \quad j+r = \text{odd}, \quad n+m = \text{odd}$$
$$r = m, \quad j+r = \text{even}, \quad n+m = \text{even}$$

$$D_{jn}^{rm} = \frac{2}{\pi\sqrt{H_n^m H_j^m}} \frac{(-1)^{\frac{j+3n-1}{2}} \sqrt{(2n+1)(2j+1)}}{(j+n+1)(j-n)} \qquad (A.6)$$
$$r = m, \quad j+r = \text{even}, \quad n+m = \text{odd}$$
$$r = m, \quad j+r = \text{odd}, \quad n+m = \text{even}$$

$$D_{jn}^{rm} = 0 \qquad (A.7)$$
$$r \neq m$$

3. Influence coefficient matrix [L]

$$\left(\tilde{L}_{jn}^{0m}\right)^c = X^m \left(\Gamma_{jn}^{0m}\right) \qquad (A.8)$$

$$\left(\tilde{L}_{jn}^{rm}\right)^c = \left[X^{|m-r|} + (-1)^k X^{|m+r|}\right]\left(\Gamma_{jn}^{rm}\right) \qquad (A.9)$$

$$\left(\tilde{L}_{jn}^{rm}\right)^s = \left[X^{|m-r|} - (-1)^k X^{|m+r|}\right]\left(\Gamma_{jn}^{rm}\right) \qquad (A.10)$$

where

$$X = \text{Tan}(\chi/2), \quad k = \min(m, r) \qquad (A.11)$$

$$\Gamma_{jn}^{rm} = \frac{\text{sign}(r-m)}{\sqrt{K_n^m K_j^m}\sqrt{(2n+1)(2j+1)}}\delta_{j,n\pm1} \qquad (A.12)$$
$$r+m = \text{odd}, \quad j+r = \text{even}, \quad n+m = \text{odd}$$
$$r+m = \text{odd}, \quad j+r = \text{odd}, \quad n+m = \text{even}$$

$$\Gamma_{jn}^{rm} = \frac{2}{\sqrt{H_n^m H_j^m}} \frac{(-1)^{\frac{n+j-2r}{2}} \sqrt{(2n+1)(2j+1)}}{(n+j)(n+j+2)\left[(n-j)^2-1\right]} \qquad (A.13)$$
$$r+m = \text{even}, \quad j+r = \text{odd}, \quad n+m = \text{odd}$$

$$\Gamma_{jn}^{rm} = \frac{8}{\pi^2 \sqrt{H_n^m H_j^m}} \frac{(-1)^{\frac{n+j-2r+2}{2}} \sqrt{(2n+1)(2j+1)}}{(n+j)(n+j+2)\left[(n-j)^2-1\right]} \qquad (A.14)$$
$$r+m = \text{even}, \quad j+r = \text{even}, \quad n+m = \text{even}$$

APPENDIX B: CONVOLUTION AND EXACT SOLUTION

The solution for simple harmonic excitation is found by applying a complex harmonic balance.

https://doi.org/10.1017/S0001924000005157 Published online by Cambridge University Press

If the pressure excitation is expressed in form

$$P = -\Phi_n^{mc}(\nu, \eta, \bar{\psi}) e^{i\omega\tau} \tag{B.1}$$

where $i = \sqrt{-1}$. The velocity will therefore be in form

$$v = \bar{v} e^{i\omega\tau} \tag{B.2}$$

Substituting Equations (B.1) and (B.2) into Equation (5) will give

$$i\omega\bar{v} - \frac{\partial \bar{v}}{\partial \xi} = \bar{\nabla}\Phi_n^{mc} \tag{B.3}$$

In scalar form Equation (B.3) becomes

$$i\omega\bar{v}_k - \frac{\partial \bar{v}_k}{\partial \xi} = \left(\Phi_n^{mc}\right)_{,k} \qquad k = z, r, \bar{\psi} \tag{B.4}$$

where $(\,)_{,k}$ denotes component in $\bar{k}$ direction. Assume the solution of Equation (A.4) is

$$\bar{v}_k = \bar{u}_k + i\bar{w}_k \qquad k = z, r, \bar{\psi} \tag{B.5}$$

Substitution of Equation (B.5) back into Equation (B.4) and separation of real and imaginary parts yield

$$\begin{cases} \omega\bar{u}_k - \dfrac{\partial \bar{w}_k}{\partial \xi} = 0 \\ \omega\bar{w}_k + \dfrac{\partial \bar{u}_k}{\partial \xi} = -\left(\Phi_n^{mc}\right)_{,k} \end{cases} \qquad k = z, r, \bar{\psi} \tag{B.6}$$

Solving $\bar{u}_k$ and $\bar{w}_k$, respectively, will give

$$\left(\Phi_n^{mc}\right)_{,z} = -\frac{1}{\nu^2 + \eta^2} \begin{pmatrix} \eta\left(1-\nu^2\right)\dfrac{\partial \Phi_n^{mc}}{\partial \nu} \\ +\nu\left(1+\eta^2\right)\dfrac{\partial \Phi_n^{mc}}{\partial \eta} \end{pmatrix} \tag{B.7}$$

If Laplace transform is used with initial conditions at $\zeta = +\infty$, which are all zeroes, it gives

$$\begin{cases} U_k(s) = -\dfrac{s}{s^2 + \omega^2} G_{nk}^m \\ W_k(s) = -\dfrac{\omega}{s^2 + \omega^2} G_{nk}^m \end{cases} \qquad k = z, r, \psi \tag{B.8}$$

where $G_{nk}^m = L\left[\left(\Phi_n^{mc}\right)_{,k}\right]$. If the convolution theorem is used to solve Equation (B.8), the components of the complex velocity can be computed by

$$\begin{cases} \bar{u}_k(\xi_0) = \int_{+\infty}^{\xi_0} \mathrm{Cos}\left(\omega(\xi_0 - \xi)\right)\left(-\Phi_n^{mc}\right)_{,k} \mathrm{d}\xi \\ \bar{w}_k(\xi_0) = \int_{+\infty}^{\xi_0} \mathrm{Sin}\left(\omega(\xi_0 - \xi)\right)\left(-\Phi_n^{mc}\right)_{,k} \mathrm{d}\xi \end{cases} \qquad k = z, r, \bar{\psi} \tag{B.9}$$

This integral can be done numerically for the convolution solution

To evaluate $\left(\Phi_n^{mc}\right)_{,k}$ in Equation (B.9) for the cosine part of a pressure distribution, the following relationship will be used

$$\frac{\partial}{\partial x} = \frac{\sqrt{\left(1-\nu^2\right)\left(1+\eta^2\right)}}{\nu^2 + \eta^2}\left(\nu\frac{\partial}{\partial \nu} - \eta\frac{\partial}{\partial \eta}\right)\mathrm{Cos}\,\bar{\psi} + \frac{1}{\sqrt{\left(1-\nu^2\right)\left(1+\eta^2\right)}}\frac{\partial}{\partial \bar{\psi}}\mathrm{Sin}\,\bar{\psi} \tag{B.10}$$

$$\frac{\partial}{\partial y} = -\frac{\sqrt{\left(1-\nu^2\right)\left(1+\eta^2\right)}}{\nu^2 + \eta^2}\left(\nu\frac{\partial}{\partial \nu} - \eta\frac{\partial}{\partial \eta}\right)\mathrm{Sin}\,\bar{\psi} + \frac{1}{\sqrt{\left(1-\nu^2\right)\left(1+\eta^2\right)}}\frac{\partial}{\partial \bar{\psi}}\mathrm{Cos}\,\bar{\psi} \tag{B.11}$$

$$\frac{\partial}{\partial z} = -\frac{1}{\nu^2 + \eta^2}\left(\eta\left(1-\nu^2\right)\frac{\partial}{\partial \nu} + \nu\left(1+\eta^2\right)\frac{\partial}{\partial \eta}\right) \tag{B.12}$$

with the relationship

$$\xi = \sqrt{(x - x_0)^2 + z^2} \tag{B.13}$$

$$\begin{cases} x = \xi\mathrm{Sin}\,\chi + x_0 \\ y = y_0 \\ z = -\xi\mathrm{Cos}\,\chi \end{cases} \tag{B.14}$$

where (x_0, y_0) is the location of point under investigation on the rotor disk. It yields

$$\begin{cases} \omega^2\bar{u}_k + \dfrac{\partial^2 \bar{u}_k}{\partial \xi^2} = -\dfrac{\partial\left(\Phi_n^{mc}\right)_{,k}}{\partial \xi} \\ \omega^2\bar{w}_k + \dfrac{\partial^2 \bar{w}_k}{\partial \xi^2} = -\omega\left(\Phi_n^{mc}\right)_{,k} \end{cases} \qquad k = z, r, \bar{\psi} \tag{B.15}$$

Noticing that, at azimuthal angle $\bar{\psi}_0$ on the surface of interest, the relationship between Cartesian coordinates and cylindrical coordinates gives

$$\frac{\partial}{\partial r} = \frac{\partial}{\partial n} = -\mathrm{Cos}\,\bar{\psi}_0\frac{\partial}{\partial x} + \mathrm{Sin}\,\bar{\psi}_0\frac{\partial}{\partial y} \tag{B.16}$$

$$\frac{\partial}{\partial \psi} = \frac{\partial}{\partial t} = \mathrm{Sin}\,\bar{\psi}_0\frac{\partial}{\partial x} + \mathrm{Cos}\,\bar{\psi}_0\frac{\partial}{\partial y} \tag{B.17}$$

and hence it gives

$$\begin{aligned} \left(\Phi_n^{mc}\right)_{,r} = &-\frac{\sqrt{\left(1-\nu^2\right)\left(1+\eta^2\right)}}{\nu^2 + \eta^2}\nu\frac{\partial \Phi_n^{mc}}{\partial \nu}\mathrm{Cos}\left(\bar{\psi}_0 - \bar{\psi}\right) \\ &+\frac{\sqrt{\left(1-\nu^2\right)\left(1+\eta^2\right)}}{\nu^2 + \eta^2}\eta\frac{\partial \Phi_n^{mc}}{\partial \eta}\mathrm{Cos}\left(\bar{\psi}_0 - \bar{\psi}\right) \\ &+\frac{1}{\sqrt{\left(1-\nu^2\right)\left(1+\eta^2\right)}}\frac{\partial \Phi_n^{mc}}{\partial \bar{\psi}}\mathrm{Sin}\left(\bar{\psi}_0 - \bar{\psi}\right) \end{aligned} \tag{B.18}$$

$$\left(\Phi_n^{mc}\right)_{,\bar{\psi}} = \frac{\sqrt{\left(1+\eta^2\right)}}{\nu^2 + \eta^2}\left(\nu\frac{\partial \Phi_n^{mc}}{\partial \nu} - \eta\frac{\partial \Phi_n^{mc}}{\partial \eta}\right)\mathrm{Sin}\left(\bar{\psi}_0 - \bar{\psi}\right) + \frac{1}{\left(1-\nu^2\right)\sqrt{\left(1+\eta^2\right)}}\frac{\partial \Phi_n^{mc}}{\partial \bar{\psi}}\mathrm{Cos}\left(\bar{\psi}_0 - \bar{\psi}\right) \tag{B.19}$$

https://doi.org/10.1017/S0001924000005157 Published online by Cambridge University Press